Plasmonics
https://doi.org/10.1007/s11468-024-02528-6

RESEARCH

Comparative Analysis of Two Different MIM Configurations of a Plasmonic Nanoantenna

Niloofar Ebrahimzadeh Esfahani[1,2] · Jaroslav Kovác Jr[1] · Giuseppe Maruccio[2,3] · Silvia Rizzato[2,3] · Soňa Kovácová[1]

Received: 25 July 2024 / Accepted: 4 September 2024

Abstract

Two plasmonic nanoantenna configurations—nanodisk and nanostrip arrays—in a metal–insulator-metal (MIM) setup were proposed, optimized, and compared by simulating their optical properties in three-dimensional models using COMSOL Multiphysics software. The optical responses, including electric field enhancement, absorption, reflection, and transmission spectra, were systematically investigated. Optimized geometrical parameters led to a significant enhancement of the electric field within the gap layers and almost perfect light absorptance for both structures. The results showed that the enhancement of the electric field depends on the polarization of the incident light. For both polarizations, the periodic circular nanodisk array showed a stronger field enhancement with an electric field enhancement factor of 6.6×10^{6} and TE polarization, and a larger absorptance of 98% at its dipole resonance wavelength, indicating the fundamental plasmonic mode. In addition, weaker resonant modes were observed in the absorptance and reflectance spectra of both nanostructures, with the nanostrips exhibiting sharper and stronger higher-order modes, making them suitable for applications requiring precise wavelength selectivity and narrow-band responses. Despite their different geometric shapes, both structures exhibited similar optimized metal film thickness and nanoparticle height, comparable modes in number and position, and identical optimized light incidence angles. Furthermore, increasing the dielectric gap layer thickness and optimizing it to a specific value revealed its ability to measure the refractive index, making it a promising candidate for sensing applications.

Keywords Nanoantenna · Nanodisk · Nanostrip · Plasmonic · Field enhancement

Introduction

Nanophotonics focuses on the enhancement and confinement of light within nanoscale geometries, plasmonics, a key area within nanophotonics has gained significant attention for its ability to control light at the nanoscale, enhancing applications in sensing, imaging, and energy harvesting [1]. Recently, the nanoparticle-on-mirror (NPOM) system has become prominent due to its capability to create highly enhanced electric field hotspots within a few nanometers by coupling a nanoparticle's dipole with its image dipole in a metal layer. The plasmonic response of NPOM systems depends on factors such as dielectric spacer thickness, incidence angle, and nanoparticle size and spacing, NPOM structures allow easy control of gap layer thickness providing advantages over conventional plasmonic structures [2–10].

A crucial step in the fabrication of NPOM structures is nanoparticle synthesis. Core-shell nanoparticles offer significant benefits over non-core-shell counterparts, notably enhancing optical absorptance and light harvesting efficiency. For example, Z, Lalegani, et al. used sol-gel synthesis to grow a 10-nm thick SiO_2 shell around 54 nm Ag nanoparticles [8, 11]. Additionally, assembling nanoparticles in specific patterns as demonstrated by Nicholas J, Greybush et al. with Au nanorods along triangular templates is essential for effective fabrication [12].

✉ Niloofar Ebrahimzadeh Esfahani
Niloofar.esfahani@stuba.sk

✉ Jaroslav Kovác Jr
Jaroslav_kovac@stuba.sk

[1] Faculty of Electrical Engineering and Information, Slovak University of Technology, Ilkovičova 3, 84104 Bratislava, Slovakia

[2] Omnics Research Group, Department of Mathematics and Physics "Ennio De Giorgi", University of Salento, Via Per Monteroni, 73100 Lecce, Italy

[3] CNR Institute of Nanotechnology and INFN Sezione Di Lecce, Via Per Monteroni, 73100 Lecce, Italy

Published online: 18 September 2024

However, metallic nanoparticles tend to aggregate, impacting their plasmonic properties and stability over time. To manage this, replacing nanoparticles with periodic metallic nanoarrays is crucial. These periodic nanostructures offer precise control over plasmonic resonances by adjusting their dimensions, thus meeting specific sensor application needs [9]. Various periodic metal nanostructures have been reported, featuring different shapes and sizes, such as nanodisks with triangular, circular, and square intersections, as well as periodic metal nanostrips with rectangular intersections [13–15]. While these nanodisks and nanostrips may appear similar in two-dimensional simulations, exhibiting identical intersections, three-dimensional simulations reveal significant differences. Therefore, studying and comparing these structures to uncover their similarities and differences is crucial for designing plasmonic structures, particularly metal-insulator-metal (MIM) nanoantennas with periodic metallic arrays. Understanding these distinctions can lead to optimized designs with enhanced performance. Metal nanostrips provide a high signal-to-noise ratio and accurate measurements due to their larger size and strong plasmonic resonances. They allow precise control over hotspots and the electric field, enhancing targeted applications. Their anisotropic nature offers design flexibility for directional responses [16–18]. Metallic nanodisk arrays, with their circular shape, exhibit unique plasmonic behavior. They are particularly useful in surface-enhanced spectroscopy, sensing, and imaging due to their strong local field enhancement. As mentioned above, despite similar 2-dimensional intersections, the 3-dimensional shapes of nanodisks and nanostrips differ, necessitating a comparative study to explore their similarities and differences for effective plasmonic structure design, especially in MIM nanoantennas.

Significant efforts have been devoted to leveraging metal-insulator-metal (MIM) structures to enhance optical absorptance and local electric field. MIM nanoantennas, which exhibit simultaneous electric and magnetic responses to incident light, are extensively used as perfect metamaterial absorbers (PMAs) in the near-infrared (NIR) and visible regions [19]. For example, Chu et al. developed a MIM-structured surface-enhanced Raman scattering (SERS) substrate with a circular nanodisk array, achieving a maximum electric field enhancement of nearly 86 [19]. Similarly, Seok et al. demonstrated an electric field enhancement of 87 in a MIM optical antenna with a nanorod dimer array [20]. However, low area fill factors reduce the density of "hot spots" and deteriorate light absorbance due to the dilution effect, typically resulting in less than 60% absorbance. Recent developments have focused on MIM PNs with sub-3 nm thick spacers to achieve strong field localizations. Lassiter et al. achieved a 90% absorbance and a calculated field enhancement of 57 using film-coupled gratings with a 2.83-nm thick spacer [21]. Huang et al. compared MIM plasmonic cavities with various nanoparticle shapes and attained a field enhancement above 100 in a nanorod cavity with a 2-nm spacer [22]. Despite these advances, achieving both strong local field enhancement ($|E|/|E_0| > 100$) and near-perfect absorbance ($> 95\%$) remains still challenging but crucial for many applications.

In the field of nanophotonics and plasmonic coupled antennas, the choice of nanoantenna types—whether plasmonic circular nanodisks, nanostrips, or bowtie nanoantennas—plays a crucial role in determining performance and suitability for specific applications [1, 23]. Depending on the application, plasmonic circular nanodisks and nanostrips offer significant advantages over bowtie nanoantennas [1]. Nanodisks, with their symmetrical shape, provide uniform light interaction and high absorptance across a range of incident angles, making them ideal for applications requiring angular tolerance and broadband absorptance [24]. Nanostrips, on the other hand, are easier to fabricate and feature directional light interaction and polarization sensitivity, which is beneficial for certain optical devices. In contrast, bowtie nanoantennas are known for their strong near-field gain and highly localized electromagnetic hotspots, which make them superior for applications such as surface-enhanced Raman spectroscopy (SERS) and nanoscale sensing [25]. As a matter of fact, the choice between these nanoantennas should be guided by the need for uniformity and broadband performance over near-field enhancement and localized field effects.

This study addresses the challenges in conventional film-coupled nanoparticle structures by designing and simulating the optical responses of two MIM plasmonic nanoantennas: periodic circular nanodisks and rectangular nanostrip arrays. Using COMSOL Multiphysics software, we optimized geometrical parameters, including the thickness of the metal film and the nanoparticle's height, as well as the incident light angle, to enhance out-of-plane plasmon coupling and light absorptance. The structures consist of a glass substrate, a gold film, and a periodic gold nanostructure (nanostrips and nanodisks) separated by an ultrathin dielectric Al_2O_3 layer. We investigated polarization dependency and measured the effect of different polarizations on electric field enhancement. Both structures exhibited three plasmonic resonance wavelengths corresponding to different modes. The periodic nano-disk array achieved stronger field enhancement and larger absorptance at its dipole resonance wavelength, while the periodic nanostrip array demonstrated sharper higher-order modes suitable for precise wavelength selectivity and narrowband responses. To complete the comparison, we measured and analyzed the sensing capabilities and sensitivities at various plasmonic modes. Both structures showed similar sensitivity at their fundamental resonance mode, with the nanostrip array displaying an extra distinct peak in its absorptance spectrum, making

it more advantageous for sensing applications. This study highlights the design and comparative analysis of periodic nanostrip and nanodisk arrays in MIM plasmonic nanoantennas. The optimized structures demonstrate significant potential for field enhancement applications and advanced sensing capabilities.

Materials and Methods

Three-dimensional electromagnetic calculations using the finite element method (FEM) in the Wave Optics module of COMSOL Multiphysics software tool are performed to design and simulate the optical response of the structures shown in Fig. 1 [26]. The reason for choosing COMSOL Multiphysics for the simulations of this work is this software is widely recognized and validated in the scientific community for its effectiveness in simulating the optical response of plasmonic and optical structures. Through extensive peer-reviewed studies and comparisons with experimental data, COMSOL has consistently demonstrated its accuracy in capturing the intricate behaviors of these systems [27–29]. The simulations rely on Maxwell's equations, integrating boundary conditions and material properties. Essential theoretical components encompass Maxwell's equations to explore the interactions between electric and magnetic fields, and the Drude or Lorentz-Drude models to characterize electromagnetic wave behavior in materials, particularly plasmonic metals.

Typically, the proposed structures consist of Au nanodisks/strips located above a metal mirror and separated by an ultrathin dielectric Al_2O_3 gap layer, as schematically shown in Fig. 1a. Gold was chosen as a plasmonic material due to its special properties. It is the metal with the second lowest loss in the visible spectrum after silver. Its superior chemical stability compared to silver makes it even more desirable for plasmonic applications. The dielectric constant or permittivity of gold plays a crucial role in determining the behavior of localized surface plasmons (LSPs). Gold exhibits a remarkably large negative real part of the permittivity in the visible and near-infrared range. This negative permittivity leads to significant resonances at certain wavelengths resulting in enhanced electromagnetic fields surrounding the nanoparticles [30]. As far as the dielectric material is concerned, Al_2O_3 has a comparatively high dielectric constant, which favors robust confinement of the electromagnetic fields within the insulator layer. This property enhances the interaction between the metal film and the nanoparticles, which intensifies the plasmonic effects. Al_2O_3 can be deposited using various methods such as atomic layer deposition (ALD) or sputtering, which allows for great flexibility in fabrication techniques. This simple deposition allows precise control over the thickness and uniformity of the dielectric layer and simplifies the production of the plasmonic structure [31].

The 60 nm thick mirror layer can be applied to a substrate using various methods such as physical vapor deposition. In contrast, the Al_2O_3 layer, which is only 5 nm thick, can only be deposited directly onto the mirror using ALD. It is important to understand that the gap between the layers in a plasmonic structure is a critical parameter that significantly affects the optical properties, including field gain, resonant wavelength, and absorption efficiency. As the gap decreases, the coupling between the metal layers strengthens, resulting in a stronger electric field in the gap region. This increased field can cause the resonance wavelength to shift to longer wavelengths (red shift) and increase absorption. However, the minimum gap size is limited by fabrication challenges and quantum tunneling effects that can occur when the gap becomes extremely narrow (typically less than 1 nm). Quantum tunneling can weaken the field enhancement and disrupt the classical plasmonic behavior, affecting the performance

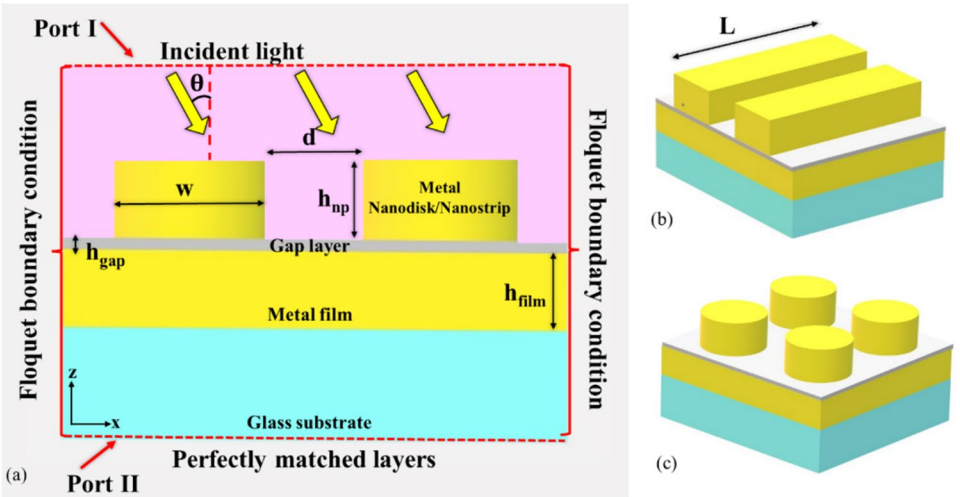

Fig. 1 **a**–**c** Schematics of the plasmonic structures: **a** 2D layout of periodic metal nanodisk/nanostrip array, **b** 3D view of the nanostrip array, and **c** 3D view of the nanodisk array. hfilm = metal film thickness, hnp = the height of the nanodisk/nano-strip, hgap = gap layer thickness, **d** = separation distance between the nanodisks/nanostrips, w = diameter/width of the nanodisk/nanostrips and L is the length of the nanostrips

of the structure. According to Wenqi Zhu et al. [32], classical models cannot accurately describe the localization of surface charges induced by an incident electromagnetic field at a thickness of less than 5 nm, and the plasmonic response is significantly altered due to the quantum properties of electrons and the associated non-local shielding. Therefore, careful optimization of the gap size is necessary to balance the improvement of optical properties with practical fabrication limits.

The height of the nanostrips and nanodisks and the thickness of the metal film were optimized to achieve maximum absorptance, and the results are discussed in the following section. The diameter and width (denoted as "*w*" in Fig. 1) of the nanodisks and nanostrips are fixed at 80 nm, while the depth of the nanostrip (*L*), which corresponds to the cell depth, is considered infinite due to the periodic Floquet boundary condition. The distance between the nanodisks and nanostrips (*d*) is 30 nm, a distance sufficient to minimize the coupling effects of localized surface plasmons in this region. As mentioned above, advanced nanofabrication techniques such as electron beam lithography can be used to fabricate these metallic periodic nanostructures. In the simulation, the illumination of port I in Fig. 1, which is perpendicular to the xy plane, and the transmission of the structure of port II. The incident light is set as a full-field electromagnetic source and is TE-polarized, while the scattered light is set as a scattered-field electromagnetic source. The designed structures have a series of inner boundaries and outer layers around the structure as perfectly matched layers. The perfectly matched layers are defined to improve the accuracy, stability, and efficiency of the simulations by effectively absorbing outgoing waves and minimizing artificial reflections at the boundaries. The periodic Floquet boundary condition (FPBC) was applied to all inner plane boundaries along the x- and y-axis to satisfy the "semi-infinite" condition for the excitation of localized surface plasmon resonance (LSPRs). This condition assumes that the model is infinite and the designed unit cell repeats periodically in the plane of the gold film (xy-plane). The model uses na = 1 for air and nb = 1.5 for the dielectric substrate. As mentioned above, the metallic part of the structure is gold and its optical properties were taken from the Optical Materials Database in the COMSOL Multiphysics software materials library (gold) (*n*, *k* 0.188–1.937 μm) [33]. The optical properties of the thin film of Al2O3 were derived from the website refractiveindex.info as a function of wavelength (Boidin et al. 2016, thin film, n 0.3–18 μm).

To gather the complete near-field spectral characteristics and identify the resonance wavelength where maximum near-field enhancement occurs, we utilize average near-field enhancement spectroscopy in this paper. This spectroscopy is achieved by averaging the volume integral of $|\boldsymbol{E}|^4/|\boldsymbol{E}_0|^4$ [34, 35]:

$$\mathrm{EF} = \frac{\iiint \frac{E^4}{E_0^4}.\mathrm{dV}}{V} \tag{1}$$

where V is the volume of the gap layer, E is the scattered electric field and E_0 is the incident electric field.

It is known that the enhancement factor (EF) of surface-enhanced Raman scattering (SERS) is approximately proportional to the fourth power of the local electric field strength |E|4/|E0|4. Consequently, the EF can be interpreted as the averaged electromagnetic enhancement factor of SERS, assuming that the adsorbed Raman probe molecules are randomly and uniformly distributed on the surface of metal nanoparticles. It is worth mentioning that in this study we evaluated the electric field enhancement using two different methods to capture different aspects of the phenomenon. The first method is based on Eq. 1, which is commonly used in SERS to quantify the EF. This approach is crucial for SERS as it emphasizes the non-linear relationship between the intensity of the electric field and the resulting signal enhancement. The second method is the use of the ratio of $|E|/|E_0|$, which is used to facilitate direct comparisons of electric field enhancement with that reported in related studies. This linear measure is more commonly used in plasmonic research for benchmarking purposes and allows us to compare our results with established findings. By using both methods, we provide a comprehensive analysis that meets the specific requirements of SERS applications and the broader context of plasmonic nanoantenna research.

To compare the sensing capability of the structures, their refractive index sensitivity (*S*) which is defined as:

$$S = \frac{\Delta\lambda}{\Delta n} \tag{2}$$

expressed in nanometers per refractive index unit (nm/RIU), where (Δλ) is the shift of the resonant peak wavelength of absorptance and (Δn) is the refractive index difference of the analyte material [36].

Result and Discussion

Optical absorptance is the fraction of incident light that is absorbed by a material or structure instead of being reflected or transmitted. In the context of plasmonic structures, absorptance is a key parameter that quantifies the efficiency with which these structures convert incident light into localized surface plasmons, resulting in enhanced electromagnetic fields and energy dissipation within the material. Figure 2 provides a detailed examination of the absorptance characteristics of plasmonic structures comprising metal nanostrip and nanodisk arrays and illustrates how the height of the nanoparticles affects absorption at different

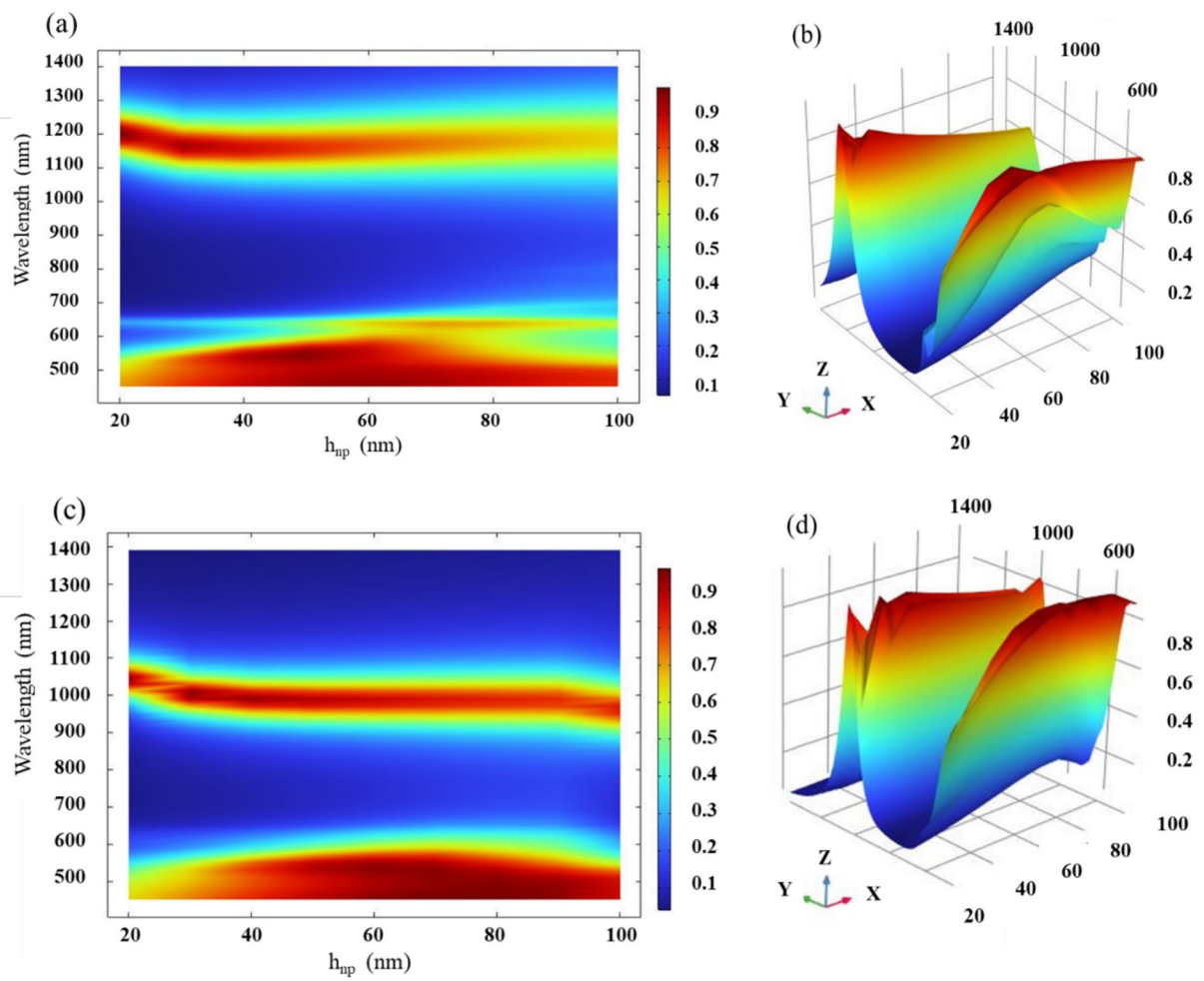

Fig. 2 **a** 2D plot showing the absorptance as a function of nanoparticle height and wavelength for the nanostrip array structure. **b** 3D visualization of absorptance variation with nanoparticle height and wavelength for nanostrip arrays, emphasizing sharpness and intensity of absorptance peaks, **c** 2D plot of absorptance as a function of nanoparticle height and wavelength for nanodisk arrays. **d** 3D visualization of absorptance variation with nanoparticle height and wavelength for nanodisk arrays, highlighting the distribution of absorptance peaks

wavelengths. The 2D plot in Fig. 2a shows the absorptance as a function of nanoparticle height (hnp) and wavelength for the nanostrip array structure. As shown, there is a pronounced absorptance peak at about 500 nm for a nanoparticle height of 50 nm and a narrow peak around 1100 nm for a height of 30 nm. In addition, a moderate increase in absorptance can be observed at 630 nm for a height of 70 nm, shown in orange. The 3D visualization in Fig. 2b shows more clearly how the absorptance varies with nanoparticle height and wavelength, highlighting the sharpness and intensity of the absorptance peaks.

The plot in Fig. 2c follows the format of part (a), but for nanodisk arrays. In this structure, a strong peak around 500 nm is observed for a nanoparticle height of 80 nm and a significant peak around 1000 nm for a height of 30 nm. The 3D representation in part (d) improves the visualization of the distribution of these absorptance peaks over the height and wavelength of the nanoparticles. The difference in the optimal height for the 500 nm peak between nanostrips and nanodisks indicates that the circular geometry of the nanodisks affects the plasmonic resonance differently, probably due to variations in field confinement and surface plasmon distribution. The comparison between Figs. 1 and 2 underline the influence of the geometry of nanostructures on the plasmonic behavior. Due to their different shapes, nanostrips, and nanodisks support different plasmonic modes that respond to the height of the nanoparticles, as shown by the shift in the optimal height for peak absorptance in each configuration.

The ability to tune absorptance peaks by adjusting the height of nanoparticles provides a versatile tool for optimizing nanoantenna designs. This tunability is particularly

valuable for applications that require precise control over the wavelength of peak absorptance, as different applications may require different spectral responses.

Figure 3 provides a revealing illustration of how the absorptance properties in plasmonic structures with metal nanostrip and nanodisk arrays are influenced by changes in metal film thickness at different wavelengths. The 2D plot in Fig. 3a shows the absorptance as a function of metal film thickness (h_{film}) in the range from 20 to 100 nm and wavelength. A clear increase in absorptance can be observed for metal films with a thickness of up to 60 nm, which is particularly noticeable at wavelengths of 1100 nm and 500 nm. For example, the absorptance at 500 nm rises sharply to around 0.85 at a film thickness of 50 nm. Beyond 60 nm, the rate of increase in absorptance decreases significantly and stabilizes around an absorptance value of 0.9, which indicates a saturation effect in the plasmonic enhancement. The maximum absorbance at 1100 nm consistently exceeds that at 500 nm, indicating a stronger plasmonic resonance at the higher wavelength. At 630 nm, there is an increase in absorptance (peak value around 0.4), which remains relatively unchanged with a further increase in metal layer thickness. The 3D plot in part (b) provides a spatial representation of these trends and visually highlights the thickness regions where the changes in absorptance are most pronounced, as well as the saturation beyond 60 nm.

Similar to part (a), the plot in part (c) shows the absorptance at different metal film thicknesses for nanodisk arrays. In this structure, the absorptance is increased at a metal layer thickness of 20 nm to 60 nm, and significantly at wavelengths of 1000 nm and 500 nm. For example, the absorptance at 1000 nm increases to about 0.88 at a thickness of 50 nm. Beyond 60 nm, similar to the nanostrips, the trend hardly changes, indicating saturation. As with the nanostrips, the absorptance maximum at around 1100 nm exceeds that at 500 nm. The 3D visualization in part d

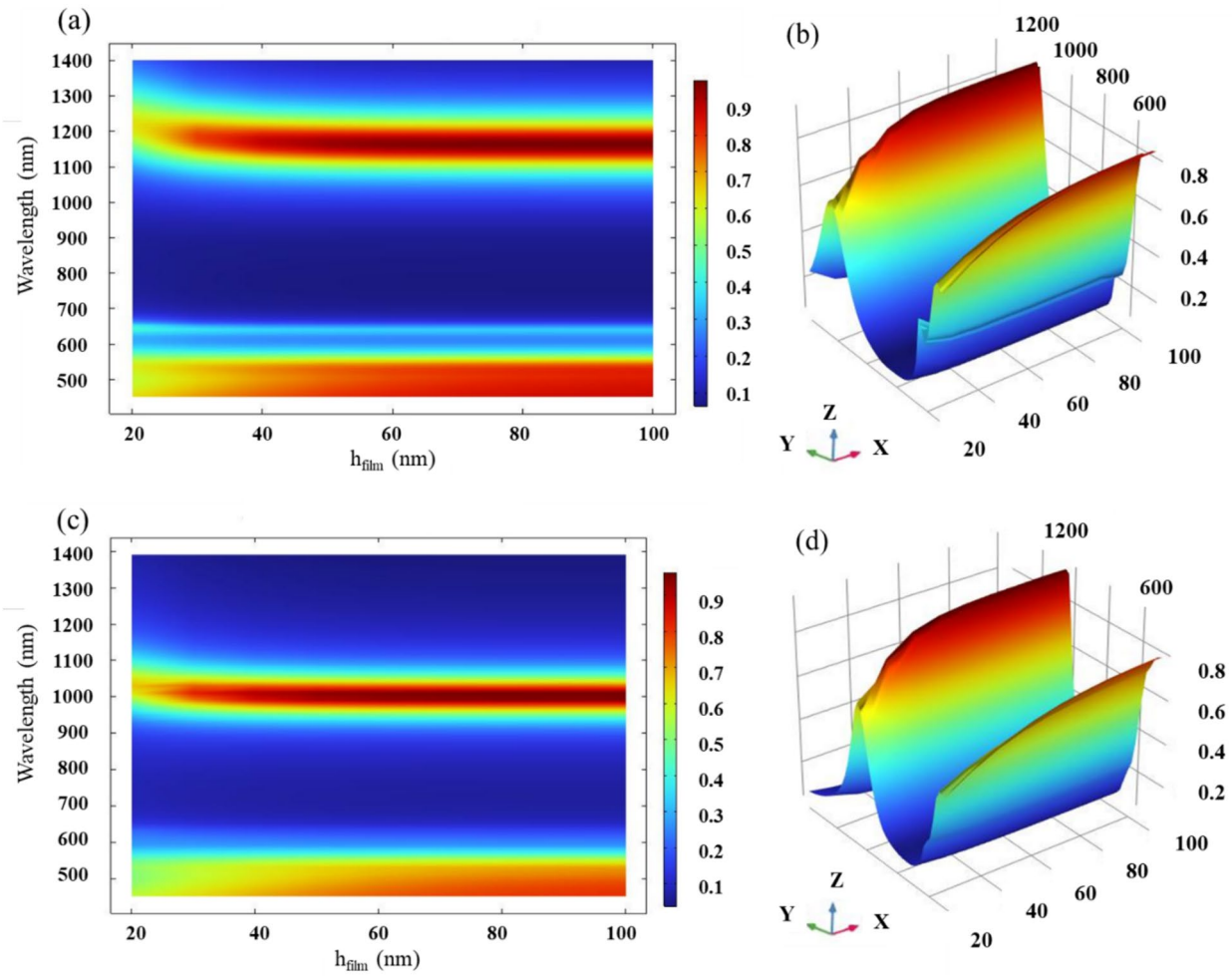

Fig. 3 **a**, **c** 2D plots depicting absorptance as a function of metal film thickness for **a** nanostrip and **c** nanodisk arrays, with notable absorptance increases up to 60 nm thickness, **b**, **d** 3D visualizations of absorptance variation with metal film thickness for **b** nanostrip, and **d** nanodisk arrays, indicating absorptance stabilization beyond 60 nm

highlights the variations of the absorptance with the thickness of the metal film and the wavelength and emphasizes the stability of the absorptance after 60 nm thickness. Figures 2 and 3 emphasize the importance of structural dimensions (nanoparticle and metal film thickness) in modulating plasmonic responses. The observed saturation of absorptance beyond 60 nm for different configurations indicates a threshold for effective plasmonic enhancement.

Figure 4 shows the 2D plot of the absorptance spectrum for both proposed structures as a function of the angle of incidence (θ, measured from the perpendicular to the xy plane) at transverse magnetic (TM) polarization. In Fig. 4a, the fundamental resonance wavelength of the structure with a nanostrip array shows no significant shift as the incident angle increases from 0 to 40°. However, it is obvious that within this range, the maximum absorptance decreases, with the strongest absorptance occurring at zero degrees. As the angle of incidence increases from 40 to 80°, a clear shift towards shorter wavelengths is observed in the resonant mode of the structure, accompanied by weaker absorptance.

As for the structure with the nanodisk array, Fig. 4b shows a similar trend to the nanostrip array, but with some differences in absorptance and resonance wavelength shift. In this case, the shift occurs at a larger wavelength around 60°. Another important point when comparing this structure with the nanostrip array is that the nanodisk array has a smaller shift in resonance wavelength and a less significant decrease in absorptance as the angle of incidence increases. Nevertheless, for both structures, the maximum absorptance is reached at an angle of incidence of zero degrees. At normal incidence angle, the nanodisk array achieves an absorptance of about 0.95 for its fundamental plasmonic mode, compared to about 0.90 for the nanostrip array. The enhanced performance of the nanodisk array can be attributed to its symmetric shape, which may provide more uniform interaction with incident light at varying angles, compared to the more directional nanostrip array. This behavior is critical for applications requiring high angular tolerance, such as in solar energy harvesting or sensing devices. These observations highlight the superior angular performance of nanodisks and emphasize the importance of considering angular sensitivity in the design of plasmonic nanoantennas. Integrating these findings with previous insights on structural parameters, such as nanoparticle height and metal film thickness, offers a comprehensive understanding of how geometry influences light interaction across different wavelengths and incident angles. For further details on the impact of incident light angle on absorptance, the reference [37] offers additional context and analysis that can enhance the reader's understanding of these effects.

The optimization of the height of the nanoparticles, the thickness of the metal film, and the angle of the incident light shows that despite the different shapes of the nanoparticles, both structures show their best performance with the same optimized parameters. This similarity could be due to their identical cross-sectional view in the xz-plane, as shown in Fig. 1a. This indicates that a two-dimensional simulation can be effectively used to optimize these parameters. However, when comparing the overall performance, the differences between the two structures become apparent and a three-dimensional simulation is required for a comprehensive evaluation. This dual approach ensures both efficiency in optimization and thoroughness in performance evaluation, paving the way for the practical use of these plasmonic structures in various technological applications.

In addition to the optimized parameters mentioned above, other factors like the length and width of the nanostrip and the diameter of the nanodisk also play an important role. For instance, in the case of nanostrips, variations in length and width alter the resonance conditions and the spatial distribution of the electromagnetic field. Increasing the length of the nanostrip generally leads to a red shift in the

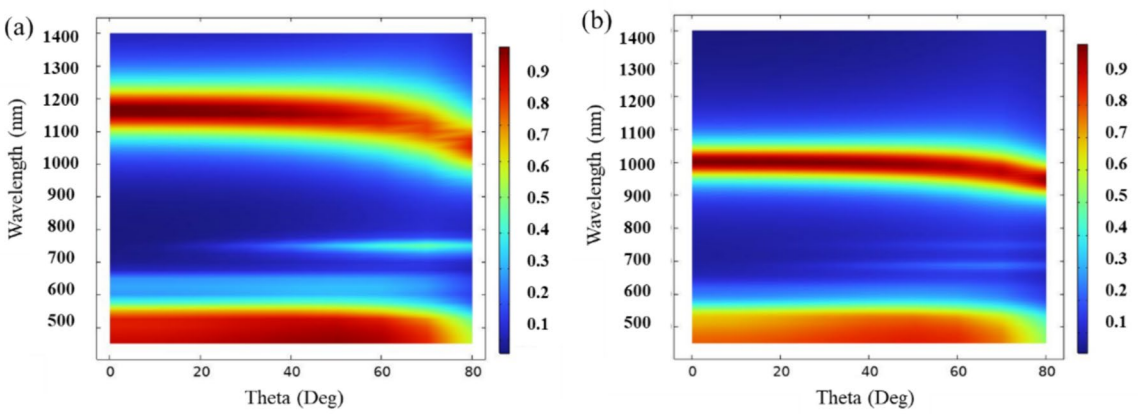

Fig. 4 2D plots depicting absorptance as a function of incident light angle for **a** nanostrip and **c** nanodisk arrays under TM polarization

resonance wavelength due to the longer path for the excitation of surface plasmons. Conversely, reducing the length tends to shift the resonance to shorter wavelengths. The width of the nanostrip also affects the resonance; a wider strip can enhance the coupling of incident light to the plasmonic modes, often resulting in stronger absorption peaks and broader resonance features. In the case of nanodisks, changes in diameter affect the plasmonic resonance and the associated absorptance spectrum. A larger diameter generally leads to a red shift in the resonance wavelength as the size of the plasmonic cavity increases, allowing for the excitation of lower-energy plasmons. Conversely, a smaller diameter results in a blue shift and potentially sharper resonance peaks. The diameter also influences the field confinement within the disk, which affects the magnitude of the absorption.

The enhancement of the electric field in plasmonic structures is of crucial importance due to its diverse applications and effects. This enhancement is particularly important in the near-field region, close to the surface of the plasmonic structures. Comparing the electric field enhancement in different plasmonic structures allows researchers and engineers to understand the underlying physics and identify optimal designs for specific applications. Figure 5a shows a comprehensive investigation of the electric field enhancement factors calculated with Eq. 1 for both structures under different polarizations (TM and TE). To visualize the electric field distribution in the gap layer at the plasmonic fundamental mode for different polarizations and to compare the electric field enhancement, the distributions of the ratio of the scattered electric field to the incident electric field for plasmonic nanostructures with nanostrip and nanodisk arrays are simulated and shown in Fig. 5b–e. It is important to note that the optimized structure parameters, including $h_{np} = 30$ nm, $h_{film} = 60$, and an incident angle of zero degrees, were used for the simulation results shown in the following sections.

Figure 5a shows clear peaks in the field enhancement factors as a function of polarization and structure type. TE polarization with nanostrip arrays exhibits a much lower enhancement factor of 1.5×10^4 at 1080 nm, indicating poor interaction with the electric field at this polarization.

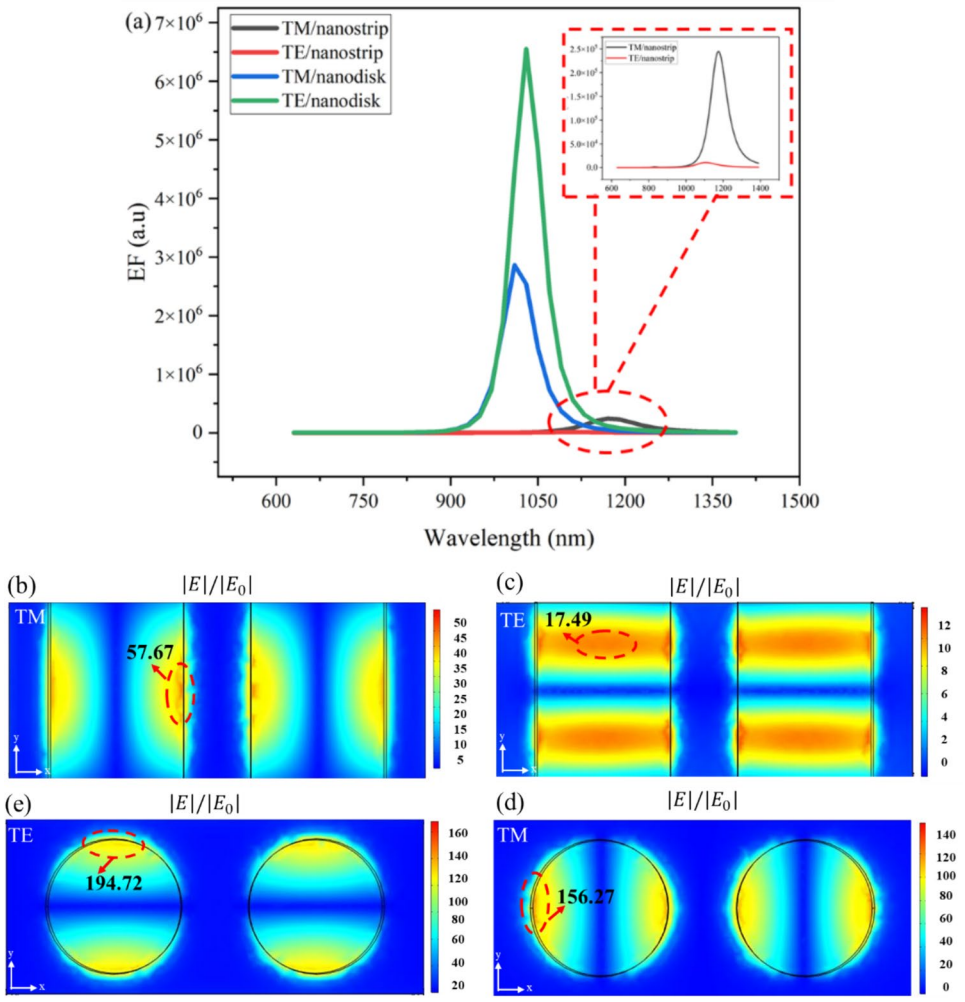

Fig. 5 **a** Electric field enhancement factors for nanostrip and nanodisk arrays under TM and TE polarizations Visualization of the electric field distribution in the gap layer for nanostrip arrays under **b** TM polarization and **c** TE polarization. Visualization of the electric field distribution for nanodisk arrays under **d** TM polarization and **e** TE polarization

In contrast, TM polarization is more effective with this structure, showing an electric field enhancement of about 2.5×10^5 at 1160 nm. The inset plot provides a focused view of the field enhancement factor for the nanostrip array under different polarizations at their dipolar resonance wavelength, highlighting the strong contrast between TM and TE modes. For nanodisk arrays, the TM polarization shows a significant peak around 1000 nm with a field enhancement factor of 2.8×10^6, while the TE polarization for the same structure shows an even higher field enhancement factor of 6.6×10^6 at 1030 nm, which is significantly larger than its TM counterpart. The observed differences in field enhancement between nanostrips and nanodisks at different polarizations are due to their different geometries and how these geometries interact with the incident electric field. The elongated shape of the nanostrips fits better with TM polarization, while the symmetric nanodisks show better performance at TE polarization due to more effective coupling and confinement of the electric field.

Figure 5b shows a strong field localization along the length of the nanostrips in TM polarization, with a maximum ratio of 57.67. In contrast, TE polarization shows a weaker and more distributed field enhancement with a maximum ratio of 17.49, which is consistent with the lower enhancement factors observed in part (a). In part (d), TM polarization for nanodisk arrays shows robust field confinement around the perimeter of the disks, although not as strong as for TE polarization. The TE polarization for nanodisk arrays in part (e) shows extremely strong field localization at the edges of the nanodisks, which is consistent with the observed high enhancement factor. The maximum ratio for TM polarizations in the nanodisk structure is 156.27, and it is 194.725 for TE polarization which is significantly higher compared to the values reported in previous studies [23, 25] for circular nanodisks and other shapes such as cubes, spheres, and rods. This result shows how the optimization of nanodisks and metal layer thickness affects the electric field enhancement. The readers are encouraged to refer to the related study [37], which provides a detailed analysis of surface charge distributions in plasmonic nanostructures.

The angular dependence of absorptance in Fig. 4 and the polarization-dependent field enhancement in Fig. 5 provide a comprehensive understanding of how these nanostructures behave under different optical conditions. Both figures illustrate the sensitivity of these structures to the orientation and polarization of the incident light, which is crucial for applications requiring precise optical manipulation. Comparing the information from Fig. 5 with the angular response from Fig. 4, it is clear that nanodisk arrays not only perform better at different angles but also exhibit better polarization-dependent field enhancement, especially at TE polarization. When choosing between nanostrip and nanodisk arrays, the polarization conditions of the operating environment should be taken into account. Nanodisks show superior performance under TE polarization and are therefore suitable for applications where such conditions prevail. Understanding the field enhancement properties under different polarizations helps tailor these nanostructures for specific applications such as sensing, where polarization effects can be used to improve sensitivity and specificity.

Figure 6 shows the absorptance, transmission, and reflectance spectra for structures with metal nanostrip

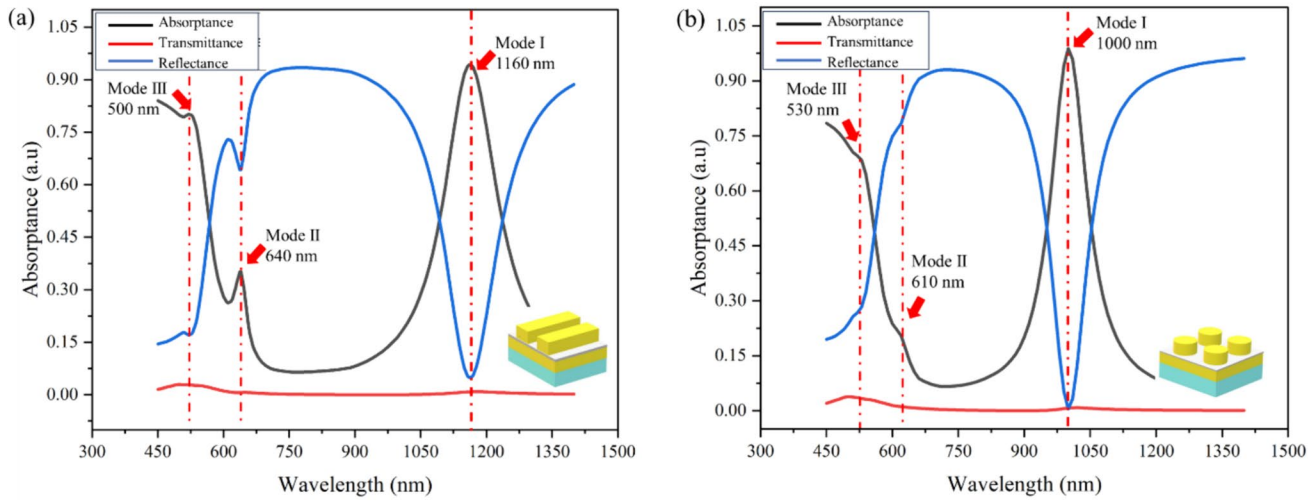

Fig. 6 Absorptance, transmittance, and reflectance spectra for **a** nanostrip and **b** nanodisk arrays under TM polarization, identifying three distinct modes and their characteristics in each structure

and nanodisk arrays under TM polarization. This analysis is crucial for understanding the optical properties and efficiency of these plasmonic structures at different wavelengths. Figure 6a shows the structure with nanostrip arrays. The graph shows three modes at different wavelengths in the visible and infrared range. Mode I, at 1160 nm, shows the highest absorptance at about 90% and low reflection below 7%, which identifies it as the fundamental plasmonic mode due to its strong absorptance and wide bandwidth. Mode II, found at 640 nm, shows an absorptance of about 35%, which is significantly lower than that of Mode I, but is characterized by a narrow bandwidth, indicating that it is a higher-order plasmonic mode. Mode III at 500 nm shows a substantial absorptance of over 75% with a broader peak compared to mode II, indicating a strong but less defined plasmonic response than the basic mode. This mode may not occur in the gap layer as it was not visible in the field enhancement factor plot in Fig. 5a. Figure 6b shows the structure with nanodisk arrays. In this structure, Mode I peaks at 1000 nm with an absorptance of over 98% and a reflectance of less than 2%, which clearly defines it as a plasmonic fundamental mode due to its exceptionally high absorptance. Mode II, found at 610 nm, has a weaker absorptance of about 20%, significantly less than Mode I, and is characterized as a higher order mode. Mode III at 530 nm has an absorptance of about 65%, which is lower than that of the nanostrip structure at a comparable mode and has a less pronounced peak.

Mode I in nanodisks has a slightly higher absorptance rate than in nanostrips, exceeding 98% at 1000 nm compared to 90% at 1160 nm in nanostrips. This suggests that nanodisks may be more efficient in the fundamental mode under TM polarization. Although the nanodisks show stronger absorptance in the fundamental modes, the nanostrips exhibit stronger and sharper absorptance in the higher order (Mode II) and Mode III modes that originate outside the gap layer, indicating different applications for these structures depending on the optical properties required. The sharpness of the peaks, especially in the higher order modes, and their specific wavelength positions are crucial for applications such as sensing or photonic devices where precise wavelength responses are required. The detailed evaluation of the absorptance, reflectance, and transmittance in the fundamental and higher-order modes provides important insights for the selection and optimization of these structures for specific applications. The strong performance of nanodisks in the fundamental modes suggests that they are suitable for applications requiring high efficiency in broad wavelengths, while the sharper and stronger responses of nanostrips in the higher-order modes make them ideal for applications requiring precise wavelength selectivity and narrowband responses.

Comparison of the plots in Figs. 5a and 6a show that Modes II and III are not visible for either structure in the field enhancement factor plot, whereas they are visible in Fig. 6a, especially for the nanostrip arrays. To gain a better insight into these missing modes in Fig. 5a, the distribution of the ratio of the scattered electric field to the incident field at different modes in the xz-plane and under TM polarization is simulated and shown in Fig. 7a, f. These visualizations are crucial for understanding the spatial properties of the electromagnetic field interactions within these structures.

As expected, Mode I, shown in Fig. 7a, d for both structures, shows a strong and uniform distribution of the electric field in the slit layer, indicating effective coupling of the localized surface plasmon resonances. This mode is the fundamental plasmonic mode and shows

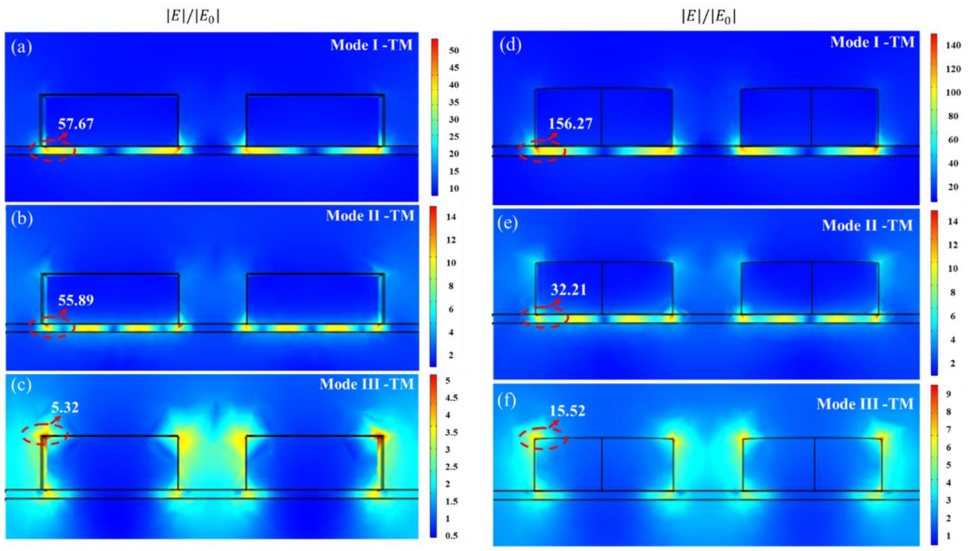

Fig. 7 **a–f** Electric field distribution visualizations for nanostrip and nanodisk arrays under TM polarization across different modes: (**a–c**) belongs to the nanostrip arrays from Mode I to Mode III and **d–f** show field distribution for the nanodisk array from Mode I to mode

significant field enhancement. Figure 7b, e shows Mode II, which has a less intense field compared to Mode I, consistent with its characterization as a higher-order mode. The field is still mainly localized in the gap layer, but with lower intensity, reflecting the narrower bandwidth and lower total energy absorptance. For Mode III, shown in Fig. 7c, f, the localization of the electric field shifts towards the edges of the nanostrips and nanodisks, especially in the upper corners. This mode shows no significant coupling in the gap layer, resulting in a lower field enhancement. The absence of a strong field in the gap layer explains its absence in the plots of field enhancement factors. These visualizations help to understand the spatial dynamics of field enhancements and their correlation with optical properties such as absorptance and reflection. This comprehensive understanding helps in tailoring these structures to specific applications where field localization and enhancement are critical, such as in enhanced spectroscopy and photonic devices.

To complete the comparison of the two structures, their sensing ability was evaluated after examining their field enhancement and near-perfect absorptance properties. In this evaluation, the refractive index (RI) of the analytical material located on the nanoparticles (instead of air) was varied from 1.33 to 1.63 and the absorptance spectrum of the structures was simulated. It is important to clarify that the actual RI detection range of the proposed structure is determined by the resonance wavelength shifts and the sensitivity of the structure. While the simulations in this study focused on the range of 1.33 to 1.63, the structure has the potential to detect RI values slightly beyond this range, depending on the specific application and sensitivity required. However, sensitivity and accuracy may decrease outside of the tested range, which is why this specific interval was emphasized in this work. Initially, no significant sensor characteristics were observed at a dielectric thickness of 5 nm. However, increasing the thickness to 10 nm led to noticeable changes in the resonance peaks for different analyte materials, as shown in Fig. 7 for both structures. The resonance peaks in plasmonic structures can shift either to longer wavelengths (red shift) or to shorter wavelengths (blue shift), depending on specific changes in the structure or in the environment. A red shift typically occurs when the coupling between the plasmonic components increases, e.g., when the distance between the metal layers decreases, resulting in a stronger electric field and a longer resonance wavelength. Conversely, a blue shift can occur when the effective refractive index of the surrounding medium decreases or when the dimensions of the nanostructures are reduced, resulting in a shorter resonance wavelength. Both types of shifts are crucial for tuning the optical properties of plasmonic structures for different applications.

Figure 8a shows that the nanostrip array structure exhibits three distinct peak shifts in the resonant wavelength, indicating its suitability for sensing applications. In contrast, although the nanodisk array structure also shows three peaks, the second peak (Mode II) is not sharp and only becomes visible at a refractive index of 1.63, making it less suitable for sensing applications compared to the nanostrip array. To obtain detailed information about the sensitivity of the individual structures in the different modes, their sensitivity was calculated using Eq. 2. The results are shown in Table 1. According to the data, the sensitivity of the two structures is similar in Modes I and III. However, in Mode II, only the nanostrip array structure shows its sensing capability. The sensitivity of these structures could be further improved by

Table 1 Comparison of the sensitivity of the structures with nanostrip and nanodisk arrays in different modes

	S (nm/RIU) Mode I	S (nm/RIU) Mode II	S (nm/RIU) Mode III
Nanostrip	300	240	150
Nanodisk	300	-	100

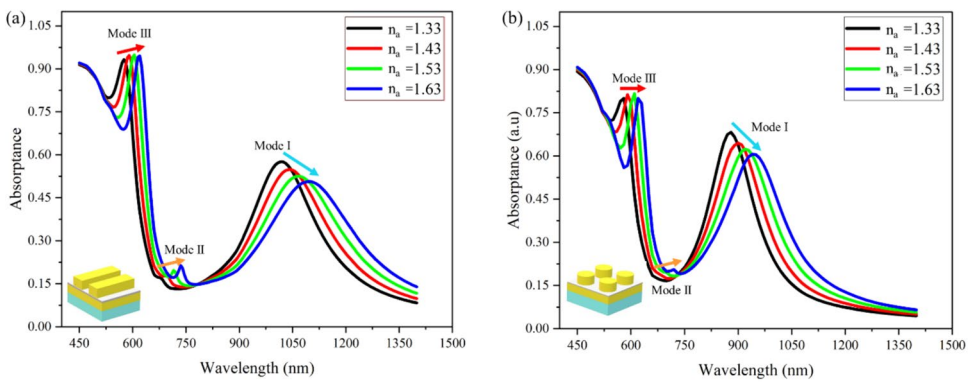

Fig. 8 Simulated absorptance spectra for **a** nanostrip and **b** nanodisk arrays with varying refractive index of the dielectric layer from 1.33 to 1.63

Table 2 Summary of field enhancement factors, optical properties, and sensing capabilities for nanostrip and nanodisk arrays under varying polarizations and modes

Nanostrip arrays	Nanodisk arrays	Comparison/key observations
- TE polarization: enhancement factor = 1.5×10^4 at 1080 nm (weak interaction) - TM polarization: enhancement factor = 2.5×10^5 at 1160 nm (better interaction)	- TM polarization: enhancement factor = 2.8×10^6 at 1000 nm (strong) - TE polarization: enhancement factor = 6.6×10^6 at 1030 nm (even stronger)	- Nanodisks show superior field enhancement under TE polarization. Nanostrips align better with TM polarization
- TM polarization: strong field localization along the nanostrips, max ratio = 57.67 - TE polarization: weaker and more distributed field, max ratio = 17.49	- TM polarization: strong field confinement along the perimeter, max ratio = 156.72 - TE polarization: extreme field localization, max ratio = 194.72	- Nanodisks show superior field localization, especially under TE polarization, outperforming other shapes
- Mode I: 90% absorptance at 1160 nm - Mode II: 35% absorptance at 640 nm - Mode III: 75% absorptance at 500 nm	- Mode I: > 98% absorptance at 1000 nm - Mode II: 20% absorptance at 610 nm - Mode III: 65% absorptance at 530 nm	- Nanodisks show better absorptance in fundamental modes, nanostrips perform better in higher-order modes
- Mode I: strong and uniform field in the gap layer - Mode II: less intense field, mostly localized - Mode III: field shifts to upper corners, weak coupling	- Mode I: strong coupling and uniform field - Mode II: weaker field intensity - Mode III: field shifts towards corners, weak in gap layer	- Mode I shows strong field coupling in both structures, Modes II and III show weaker field localization
- Peak shifts: 3 distinct resonance wavelength shifts with refractive index (RI) from 1.33 to 1.63 - Sensitivity: Mode I = 300 nm/RIU, Mode II = 240 nm/RIU, mode III = 150 nm/RIU	- Peak shifts: 3 peaks, mode II lacks sharpness - Sensitivity: mode I = 300 nm/RIU, Mode II = N/A, Mode III = 100 nm/RIU	- Nanostrips exhibit sharper and stronger shifts in resonance peaks, making them more suitable for sensing

optimizing other parameters, such as the spacing and diameter of the nanoparticles, or by increasing the dielectric layer thickness beyond 10 nm. The choice of a layer thickness of 10 nm for these structures is of strategic importance: it is thin enough to ensure strong field enhancement in the gap layer and at the same time thick enough to enable sensing capability. This balance is crucial to achieve both high field enhancement and effective sensing performance.

Table 2 summarizes the key findings related to the field enhancement, optical properties, and sensing capabilities of nanostrip and nanodisk arrays. It demonstrates that nanodisk arrays perform better in field enhancement under TE polarization, while nanostrip arrays exhibit sharper absorptance peaks in higher-order modes and better detection performance, especially in Mode II. This summary emphasizes the importance of selecting the appropriate nanostructure based on the desired optical performance and sensing application.

Table 3 provides a comparative analysis of performance metrics for different plasmonic nanostructures, highlighting the differences in electric field enhancement, absorptance, sensing capabilities, and resonance wavelengths reported in recent studies. This comparison illustrates the performance of the nanostructures in the current study compared to other studies. The nanodisk arrays in this study exhibit one of the highest field enhancement factors at TE polarization (6.6×10^6), surpassing the values reported by Sherry et al. [38] and Qiao et al. [39]. In addition, the nanodisk structures achieve a near-perfect absorptance of 98%, which is higher than the 96% absorptance found for nanostars by Gomez et al. [40]. The sensitivity of the nanostrip arrays in mode I (300 nm/RIU) is comparable to the sensitivity of nanocubes reported by Liu et al. [23], indicating competitive sensing capabilities. Overall, the results of the current study show strong performance in electric field enhancement, absorptance, and sensing capability, making it the leading work in the field of plasmonics. Future research could explore variations in nanoparticle geometry and material composition to further enhance the sensitivity and performance of these plasmonic structures. Additionally, investigating the effects of different dielectric materials and their thicknesses on the overall optical and sensing properties could provide deeper insights and lead to more optimized designs. The ultimate goal is to develop highly sensitive and efficient plasmonic sensors tailored for specific applications, ranging from biochemical sensing to advanced photonic devices.

Conclusion

In conclusion, this study conducted a comparative analysis of two plasmonic nanoantenna configurations—nanodisk and nanostrip arrays—within a metal-insulator-metal

Table 3 Comparison of plasmonic nanostructures across studies

Study	Nanostructure type	Material	Polarization	Electric field enhancement factor	Absorptance	Sensing capability (nm/RIU)	Resonance wavelength (nm)
Current study	Nanostrip and nanodisk arrays	Gold	TE/TM	6.6×10^6 (TE, nanodisk)	98% (nanodisk)	300 (Mode I, nanostrip)	1160 (nanostrip), 1000 (nanodisk)
[38]	Nanorods	Silver	TM	5.0×10^5	85%	220	840
[39]	Nanospheres	Gold	TE	1.2×10^6	95%	280	910
[23]	Nanocubes	Silver	TM	3.8×10^6	90%	300	1200
[24]	Nanodisks	Aluminum	TE	4.5×10^6	88%	250	980
[41]	Nanorings	Gold	TM	2.5×10^6	92%	290	1050
[40]	Nanostars	Silver	TE	7.1×10^6	96%	320	990
[42]	Nanoshells	Gold	TM	4.0×10^5	80%	–	–

(MIM) setup. Using COMSOL Multiphysics software, the optical properties of these structures were simulated to optimize and compare their potential applications for enhancing light absorptance and electric field strength. Optimization of the nanoparticle height revealed that both structures exhibit their strongest absorptance at their fundamental plasmonic mode at a height of approximately 30 nm. However, their maximum absorptance at other modes occurred at different heights. Similar results were observed when optimizing the thickness of the metal film, with both structures showing the strongest absorptance at their fundamental modes at a thickness of 60 nm. Comparing the absorptance of the structures under TM polarization, the nanodisk arrays achieved a maximum absorptance of over 98% at 1000 nm (Mode I), while the nanostrip arrays reached a maximum absorptance of 90% at 1160 nm. This indicates that nanodisk arrays are more efficient at fundamental mode absorptance under TM polarization. On the other hand, a comparison of their field enhancement factors under different polarizations shows that under TE polarization, the nanodisk arrays demonstrated a significant field enhancement factor of 6.6×10^6 at 1030 nm, surpassing the nanostrip arrays, which showed a maximum field enhancement factor of 2.5×10^5 at 1160 nm under TM polarization. The angular dependence of absorptance revealed that nanodisk arrays had higher absorptance values compared to nanostrip arrays at different angles of incidence. This characteristic, along with superior polarization-dependent field enhancement, suggests that nanodisk arrays are more suitable for applications requiring high angular tolerance and sensitivity to polarization. When the thickness of the dielectric gap layer was increased to 10 nm, both structures demonstrated the capability for refractive index sensing. Their sensitivity at different modes shows that both structures have similar sensitivity at their fundamental resonance mode. However, the nanostrip array displayed an additional clear peak on its absorptance spectrum, making it more suitable for sensing applications. Overall, the results indicate that nanodisk arrays are preferable for applications demanding strong field enhancement and broad wavelength absorptivity, while nanostrip arrays are advantageous for applications needing precise wavelength selectivity and narrowband responses. Additionally, with an appropriate gap layer thickness, both structures exhibit sensing properties, making them versatile for various applications. Future research could further optimize these structures by exploring variations in nanoparticle geometry, material composition, and dielectric layer thickness to enhance their performance in specific applications, ranging from biochemical sensing to advanced photonic devices.

Acknowledgements We would like to extend our sincere gratitude to Dr. Behzad Sadeghi for his invaluable scientific support and guidance throughout this research. His expert advice and constructive feedback have been instrumental in shaping this study. Additionally, we are deeply appreciative of his assistance with the submission process, which ensured that our work was presented effectively and efficiently.

Author Contributions Conceptualization: Niloofar Ebrahimzadeh Esfahani, Jaroslav Kovác, Giuseppe Maruccio, Silvia Rizzato, Soňa Kovácová. Methodology: Niloofar Ebrahimzadeh Esfahani, Silvia Rizzato, Soňa Kovácová. Software: Niloofar Ebrahimzadeh Esfahani. Validation: Niloofar Ebrahimzadeh Esfahani, Jaroslav Kovác, Giuseppe Maruccio, Soňa Kovácová. Formal Analysis: Niloofar Ebrahimzadeh Esfahani, Soňa Kovácová. Investigation: Niloofar Ebrahimzadeh Esfahani, Jaroslav Kovác, Giuseppe Maruccio. Resources: Jaroslav Kovác, Giuseppe Maruccio. Data Curation: Niloofar Ebrahimzadeh Esfahani, Jaroslav Kovác, Giuseppe Maruccio, Silvia Rizzato. Writing - Original Draft: Niloofar Ebrahimzadeh Esfahani, Soňa Kovácová. Writing - Review & Editing: Niloofar Ebrahimzadeh Esfahani, Jaroslav Kovác, Giuseppe Maruccio. Visualization: Niloofar Ebrahimzadeh Esfahani, Silvia Rizzato, Soňa Kovácová. Supervision: Jaroslav Kovác, Giuseppe

Maruccio. Project Administration: Jaroslav Kovác, Giuseppe Maruccio. Funding Acquisition: Jaroslav Kovác.

Funding Open access funding provided by The Ministry of Education, Science, Research and Sport of the Slovak Republic in cooperation with Centre for Scientific and Technical Information of the Slovak Republic. This work was supported by project APVV 20 0437 from the Slovak research and development agency of the Ministry of Education, Science, Research and Sport of the Slovak Republic.

Data Availability No datasets were generated or analysed during the current study.

Declarations

Competing Interests The authors declare no competing interests.

References

1. Jamil S, Farooq W, Khalil UK, Kazmi SZA, Khan AD, Iqbal J (2021) Transition from conventional lasers to plasmonic spasers: a review. Appl Phys A 127:1–19
2. Li Y, Hu H, Jiang W, Shi J, Halas NJ, Nordlander P, Zhang S, Xu H (2020) Duplicating plasmonic hotspots by matched nanoantenna pairs for remote nanogap enhanced spectroscopy. Nano Lett 20(5):3499–3505
3. Gurbatov S, Vitrik O, Kulchin Y, Kuchmizhak A (2018) Mapping the refractive index with single plasmonic nanoantenna. Sci Reps 8(1):3861
4. Zheng P, Kasani S, Wu N (2019) Converting plasmonic light scattering to confined light absorption and creating plexcitons by coupling a gold nano-pyramid array onto a silica–gold film. Nanoscale horizons 4(2):516–525
5. Ebrahimzadeh Esfahani N, Kováč J Jr, Kováčová S, Feiler M (2023) Plasmonic Properties of the Metal Nanoparticles (NPs) on a Metal Mirror Separated by an Ultrathin Oxide Layer. Photonics 10(1):78
6. Barreda A, Mercadé L, Zapata-Herrera M, Aizpurua J, Martínez A (2022) Hybrid photonic-plasmonic cavity design for very large purcell factors at telecommunication wavelengths. Phys Rev Appl 18(4):044066
7. Baumberg JJ, Aizpurua J, Mikkelsen MH, Smith DR (2019) Extreme nanophotonics from ultrathin metallic gaps. Nat Mater 18(7):668–678
8. Lin L, Zheng Y (2015) Optimizing plasmonic nanoantennas via coordinated multiple coupling. Sci Rep 5(1):14788
9. Nicolas R, Lévêque G, Marae-Djouda J, Montay G, Madi Y, Plain J, Herro Z, Kazan M, Adam P-M, Maurer T (2015) Plasmonic mode interferences and Fano resonances in Metal-Insulator-Metal nanostructured interface. Sci Rep 5(1):14419
10. Chao C-TC, Kooh MRR, Lim CM, Thotagamuge R, Mahadi AH, Chau Y-FC (2023) Visible-range multiple-channel metal-shell rod-shaped narrowband plasmonic metamaterial absorber for refractive index and temperature sensing. Micromachines 14(2):340
11. Lalegani Z, Ebrahimi SS, Hamawandi B, La Spada L, Batili H, Toprak M (2022) Targeted dielectric coating of silver nanoparticles with silica to manipulate optical properties for metasurface applications. Mater Chem Phys 287:126250
12. Greybush NJ, Pacheco-Peña V, Engheta N, Murray CB, Kagan CR (2019) Plasmonic optical and chiroptical response of self-assembled Au nanorod equilateral trimers. ACS Nano 13(2):1617–1624
13. Khalil UK, Farooq W, Iqbal J, Ul Abideen Kazmi SZ, Khan AD, Ur Rehman A, Ayub S (2021) Design and optimization of bowtie nanoantenna for electromagnetic field enhancement. Eur Phys J Plus 136:1–13
14. Chou Chau Y-F, Chou Chao C-T, Rao J-Y, Chiang H-P, Lim CM, Lim RC, Voo NY (2016) Tunable optical performances on a periodic array of plasmonic bowtie nanoantennas with hollow cavities. Nanoscale Res Lett 11:1–9
15. Chau Y-FC, Jiang J-C, Chao C-TC, Chiang H-P, Lim CM (2016) Manipulating near field enhancement and optical spectrum in a pair-array of the cavity resonance based plasmonic nanoantennas. J Phys D Appl Phys 49(47):475102
16. Liu D, Chen L, Wu X, Liu F (2020) Terahertz composite plasmonic slabs based on double-layer metallic gratings. Opt Express 28(12):18212–18223
17. Chen L-S, Wang Z-Y, Bai R-Y, Wang Y, Wang X (2019) Design and analysis of a Ag rhombus nanoparticle film-coupled plasmonic nanostructure. ACS Omega 4(12):14759–14764
18. Gu P, Wan M, Wu W, Chen Z, Wang Z (2016) Excitation and tuning of Fano-like cavity plasmon resonances in dielectric–metal core–shell resonators. Nanoscale 8(19):10358–10363
19. Chu Y, Banaee MG, Crozier KB (2010) Double-resonance plasmon substrates for surface-enhanced Raman scattering with enhancement at excitation and stokes frequencies. ACS Nano 4(5):2804–2810
20. Seok TJ, Jamshidi A, Kim M, Dhuey S, Lakhani A, Choo H, Schuck PJ, Cabrini S, Schwartzberg AM, Bokor J (2011) Radiation engineering of optical antennas for maximum field enhancement. Nano Lett 11(7):2606–2610
21. Lassiter JB, Chen X, Liu X, Ciracì C, Hoang TB, Larouche S, Oh S-H, Mikkelsen MH, Smith DR (2014) Third-harmonic generation enhancement by film-coupled plasmonic stripe resonators. ACS Photonics 1(11):1212–1217
22. Huang S, Ming T, Lin Y, Ling X, Ruan Q, Palacios T, Wang J, Dresselhaus M, Kong J (2016) Ultrasmall mode volumes in plasmonic cavities of nanoparticle-on-mirror structures. Small 12(37):5190–5199
23. Liu Y, Wu S-H, Du X-Y, Sun J-J (2021) Plasmonic Ag nanocube enhanced SERS biosensor for sensitive detection of oral cancer DNA based on nicking endonuclease signal amplification and heated electrode. Sens Actuators, B Chem 338:129854
24. Katyal J, Soni R (2013) Size-and shape-dependent plasmonic properties of aluminum nanoparticles for nanosensing applications. J Mod Opt 60(20):1717–1728
25. Sbeah ZA, Adhikari R, Sorathiya V et al (2023) A review on metamaterial sensors based on active plasmonic materials. Plasmonics 18:1619–1638
26. https://www.comsol.com/
27. Saini RK, Sharma AK, Agarwal A, Prajesh R (2022) Near field FEM simulations of plasmonic gold nanoparticle based

SERS substrate with experimental validation. Mater Chem Phys 287:126288
28. Kluczyk K, Jacak W (2016) Damping-induced size effect in surface plasmon resonance in metallic nano-particles: comparison of RPA microscopic model with numerical finite element simulation (COMSOL) and Mie approach. J Quant Spectrosc Radiat Transfer 168:78–88
29. Tsoulos T, Han L, Weir J, Xin H, Fabris L (2017) A closer look at the physical and optical properties of gold nanostars: An experimental and computational study. Nanoscale 9(11):3766–3773
30. West PR, Ishii S, Naik GV, Emani NK, Shalaev VM, Boltasseva A (2010) Searching for better plasmonic materials. Laser Photonics Rev 4(6):795–808
31. Singh AK, Hennig RG, Davydov AV, Tavazza F (2015) Al2O3 as a suitable substrate and a dielectric layer for n-layer MoS2. Appl Phys Lett 107(5)
32. Zhu W, Esteban R, Borisov AG, Baumberg JJ, Nordlander P, Lezec HJ, Aizpurua J, Crozier KB (2016) Quantum mechanical effects in plasmonic structures with subnanometre gaps. Nat Commun 7(1):1–14
33. Johnson PB, Christy RW (1972) Optical constants of the noble metals. Phys Rev B 6(12):4370
34. Jiang N, Zhuo X, Wang J (2017) Active plasmonics: principles, structures, and applications. Chem Rev 118(6):3054–3099
35. Li JF, Huang YF, Ding Y, Yang ZL, Li SB, Zhou XS, Fan FR, Zhang W, Zhou ZY, Wu DY (2010) Shell-isolated nanoparticle-enhanced Raman spectroscopy. Nature 464(7287):392–395
36. Dormeny AA, Sohi PA, Kahrizi M (2020) Design and simulation of a refractive index sensor based on SPR and LSPR using gold nanostructures. Results Phys 16:102869
37. Chau Y-FC, Chao C-TC, Chiang H-P, Lim CM, Voo NY, Mahadi AH (2018) Plasmonic effects in composite metal nanostructures for sensing applications. J Nanopart Res 20:1–13
38. Sherry LJ, Chang S-H, Schatz GC, Van Duyne RP, Wiley BJ, Xia Y (2005) Localized surface plasmon resonance spectroscopy of single silver nanocubes. Nano Lett 5(10):2034–2038
39. Qiao L, Wang D, Zuo L, Ye Y, Qian J, Chen H, He S (2011) Localized surface plasmon resonance enhanced organic solar cell with gold nanospheres. Appl Energy 88(3):848–852
40. Reyes Gomez F, Rubira RJ, Camacho SA, Martin CS, Da Silva RR, Constantino CJ, Alessio P, Oliveira ON Jr, Mejía-Salazar JR (2018) Surface plasmon resonances in silver nanostars. Sensors 18(11):3821
41. Tsai C-Y, Lin J-W, Wu C-Y, Lin P-T, Lu T-W, Lee P-T (2012) Plasmonic coupling in gold nanoring dimers: Observation of coupled bonding mode. Nano Lett 12(3):1648–1654
42. Tuersun P (2016) Optimizing the figure of merit of gold nanoshell-based refractive index sensing. Optik 127(1):250–253